Focused mid-crustal magma intrusion during continental break-up in Ethiopia

Kevin Wong[1*], David Ferguson[1], Penny Wieser[2], Daniel Morgan[1], Marie Edmonds[3], Amdemichael Zafu Tadesse[4], Gezahegn Yirgu[5], Jason Harvey[1], and Samantha Hammond[6]

[1]School of Earth and Environment, University of Leeds, Leeds LS2 9JT, United Kingdom
[2]Earth and Planetary Science, University of California, Berkeley, CA 94720-4767, United States of America
[3]Centre for the Observation and Modelling of Earthquakes, Volcanoes and Tectonics (COMET), Department of Earth Sciences, University of Cambridge, Cambridge CB2 3EQ, United Kingdom
[4]Department of Geosciences, Environment and Society, Université Libre de Bruxelles (ULB), 50 B-1050 Bruxelles, Belgium
[5]School of Earth Sciences, Addis Ababa University, P. O. Box 1176 Addis Ababa, Ethiopia
[6]School of Environment, Earth and Ecosystems Sciences, The Open University, Milton Keynes MK7 6AA, United Kingdom

Key Points:

- We determine magma storage conditions in the Main Ethiopian Rift through geochemical analysis of olivine-hosted melt inclusions.
- Volatile saturation barometry reveals that basaltic melts are focused at 10–15 km depth in the Ethiopian crust.
- Geochemical heterogeneity in melt inclusions suggests that magma storage is likely to occur in semi-discrete sills.

*Current address, Department of Biological, Geological, and Environmental Sciences (BiGeA), Alma Mater Studiorum Università di Bologna, Piazza di Porta San Donato 1, 40126, Bologna, Italy

Corresponding author: Kevin Wong, kevin.wong@unibo.it

Abstract

Significant volumes of magma are intruded into the crust during continental break-up, which can influence rift evolution by altering thermo-mechanical structure of the crust and thereby its response to extensional stresses. Rift magmas additionally feed surface volcanic activity and can be globally significant sources of tectonic CO_2 emissions. Understanding how magmatism may affect rift development requires knowledge on magma intrusion depths in the crust. Here, using data from olivine-hosted melt inclusions, we investigate magma dynamics for basaltic intrusions in the Main Ethiopian Rift (MER). We find evidence for a spatially focused zone of magma intrusion at the MER upper-lower crustal boundary (10-15 km depth), consistent with geophysical datasets. We propose that ascending melts in the MER are intruded over this depth range as discrete sills, likely creating a mechanically weak mid-crustal layer. Our results have important implications for how magma addition can influence crustal rheology in a maturing continental rift.

Plain Language Summary

Continental rifting, the break-up of continents to form new ocean basins, is a key component in the tectonic cycle that affects Earth's surface environment. The rifting process is aided by magmatic activity in its final stages, which weakens the crust by heating it. This is believed to facilitate present-day rifting in Ethiopia, where we can find rift-related volcanoes. Where melts are stored in the rifting crust will determine how heat is distributed, and therefore how the physical properties of the crust will be altered. Here we analyse melt inclusions, small pockets of precursor magmas trapped in crystals. Because melt inclusions are trapped at depth they record key geochemical information about the conditions magmas experience as they enter the crust from the mantle. By considering the concentrations of CO_2 and H_2O in our melt inclusions we demonstrate that magmas are focused in a 10–15 km zone in the rifting Ethiopian crust. The diverse geochemistry of our melt inclusions additionally suggests that magmas do not substantially mix together in the crust, and are likely to be stored within non-interacting magmatic bodies. This study therefore provides new insights into how melts are stored in the Ethiopian crust before volcanic eruptions.

1 Introduction

Continental rifting involves the rupture of strong continental lithosphere to form new ocean basins. Evidence from active continental rifts and passive margins suggests that continental break-up often involves intrusion of substantial volumes of magma into the rifting crust (e.g., White et al., 2008; Bastow et al., 2011; Bastow & Keir, 2011). These magmas can accommodate extension via dyke intrusion and, depending on their distribution in space and time, may alter the thermo-mechanical structure of the crust (e.g., Buck, 2006; Daniels et al., 2014; Lavecchia et al., 2016; Muluneh et al., 2020). Determining where and how intruded melts accumulate during rift development is therefore crucial for understanding how the rheology and density structure of the crust evolves with progressive rifting, which in turn has a strong influence on how the crust responds to far-field extensional stresses during non-magmatic and magmatic rifting regimes (e.g., Bialas et al., 2010; Tetreault & Buiter, 2018; Oliveira et al., 2022).

Although the syn-rift interplay between magmatism and tectonics is a key ingredient in facilitating continental break-up (e.g., Thybo & Nielsen, 2009; Bastow & Keir, 2011), observational constraints on the depths of basaltic intrusion in active rifts obtained through petrology and geochemistry remain limited. While geophysical observations can infer depths of intrusion and storage of crustal melts (e.g., seismicity concurrently triggered during emplacement; Keir et al., 2006; Ebinger et al., 2008), only petrological observations, obtained from basaltic materials derived directly from the intruding melts

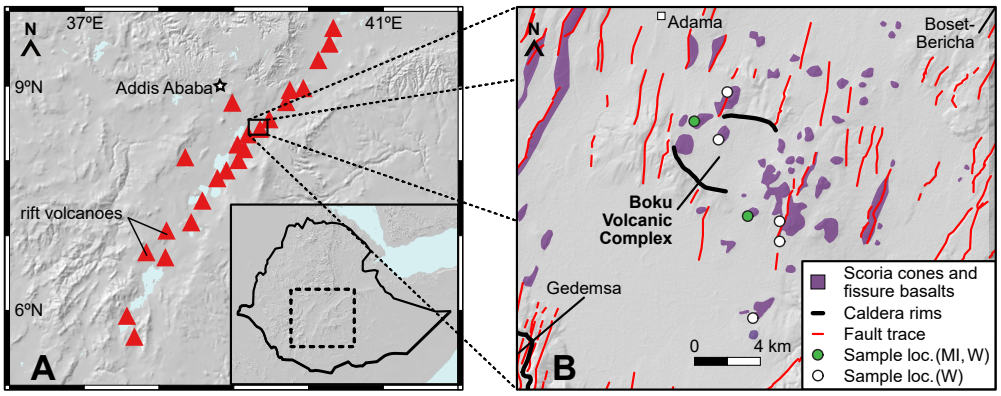

Figure 1. A. The location of the Boku Volcanic Complex in the MER. B. Simplified geological map of Boku, with olivine-hosted melt inclusion (MI) and whole-rock (W) sample localities shown. Digital elevation models are GTOPO30 (A) and SRTM (B). Volcano locations in subfigure A are obtained from the Global Volcanism Program, Smithsonian Institution (`https://volcano.si.edu/`).

themselves, can provide first-hand evidence of the magmatic conditions associated with crustal emplacement.

The Main Ethiopian Rift (MER), comprising the northernmost sector of the East African Rift system (EARS), provides a natural laboratory to examine the interplay between rift geodynamics and magmatic intrusion. This late-stage continental rift, which bridges the large fault-bound grabens of the Kenyan Rift and inferred incipient seafloor spreading in Afar (Figure 1A), has been extensively studied through multiple geophysical approaches (e.g., Bastow et al., 2011). These studies suggest that significant magma intrusion has occurred in the MER lithosphere, focused under ∼20 km-wide and ∼60 km-long magmatic-tectonic segments (e.g., Bastow et al., 2011), where as much as half of the crustal volume may comprise new igneous material (Maguire et al., 2006; Daniels et al., 2014). The compositional and thermal effects of magma intrusion may modify the response of the Ethiopian crust to extension, determining where and how strain is localized as rifting proceeds (e.g., Bastow & Keir, 2011; Lavecchia et al., 2016). Furthermore, degassing of intruded melts during and after emplacement contributes to the significant diffuse CO_2 fluxes measured in the MER (Hunt et al., 2017).

In this study we use petrological methods to investigate the storage depths and compositional diversity of intruded basaltic magmas in the northern MER. Our constraints on magma intrusion conditions are derived from analysis of olivine-hosted silicate melt inclusions (MIs), which are small pockets of quenched magma trapped within growing crystals during crustal magma storage (e.g., Wallace et al., 2021). Unlike erupted lavas, MIs can preserve magmatic volatile contents (e.g., CO_2, H_2O etc., Wallace et al., 2021), allowing volatile saturation pressures, and therefore magmatic storage depths, to be determined (e.g., Ghiorso & Gualda, 2015). Of particular importance is the volatile species CO_2, which degases strongly with decreasing pressure in basaltic magmas (e.g., Dixon et al., 1995). Continental rifts, including the MER, are known to be significant sources of passively degassing magmatic CO_2 (Lee et al., 2016; Foley & Fischer, 2017; Hunt et al., 2017). By considering the total CO_2 in MIs, entrapped within both glass and bubble, we provide new well-constrained petrological estimates of basaltic intrusion pressures in the MER.

2 Materials and Methods

Our samples are scoriae from the Boku Volcanic Complex, a Quaternary monogenetic basaltic cone field located in the northern MER (Figure 1B Tadesse et al., 2019). Littering the remnants of a collapsed ∼500 ka caldera, the later-stage ∼200 ka basaltic cones and fissure flows of Boku are associated with adjacent faults which are sub-parallel to the strike of the MER (Figure 1; Rooney et al., 2011; Tadesse et al., 2019). Quarries provide access into the interiors of cones, where fresh glassy basaltic scoria can be sampled.

Olivine crystals from two Boku cones (Figure 1), picked from disaggregated scoria, were characterized for MIs, individually polished to 0.25 μm grade on glass slides to expose MIs, and mounted in epoxy resin. We have measured the compositions of 40 MIs (full methods in Supporting Information). 27 of these MIs contain CO_2-rich vapor bubbles, which form from post-entrapment changes in pressure, volume and temperature (e.g., Moore et al., 2015; Maclennan, 2017). Bubbles can host a significant fraction of the MI CO_2 budget (e.g., Hartley et al., 2014; Wieser et al., 2021). To estimate the total CO_2 in MIs, essential for accurate barometry, 18 MIs were additionally assessed for shrinkage bubble CO_2 density using Raman spectroscopy. Our approach differs from previous studies considering MIs from the EARS in this regard, which have opted to either a) experimentally rehomogenize the bubble (Head et al., 2011; Hudgins et al., 2015), b) use CO_2 equation of state methods (Rooney et al., 2022), or c) select MIs without vapor bubbles wherever possible (Field, Barnie, et al., 2012; Field, Blundy, et al., 2012; A. Donovan et al., 2017; Iddon & Edmonds, 2020). The primary advantage of our approach is the direct measurement of bubble CO_2 without making assumptions concerning bubble cooling history and post-entrapment processes or experimentally modifying the MI glass composition, which will introduce uncertainties that are difficult to assess and quantify (Rasmussen et al., 2020; Wieser et al., 2021). In addition, by selecting bubble-hosting MIs we avoid biases towards magmatic conditions that favor bubble-free MIs, which may not be representative of crustal melt storage. By doing so, we provide a robust estimate of total CO_2 in an MI, which can be used to determine crustal melt storage pressures.

After Raman spectroscopy, all MIs were analysed for trace and volatile elements in the glass phase by SIMS. This was followed by EPMA to assess major element compositions of MI glass, carrier melt, and host olivine crystals. MI compositions were corrected for post-entrapment crystallization (PEC) using Petrolog3 software (Danyushevsky & Plechov, 2011, full details in Supporting Information). The total CO_2 of MIs is calculated by mass balance using the CO_2 measured in the bubble and MI glass (e.g., Hartley et al., 2014). To complement the MI compositional dataset, we have additionally assessed the major and trace element whole-rock compositions of basalts collected from several Boku scoria cones and fissure flows using XRF and solution ICP-MS respectively. All standards and geochemical data are presented in Supporting Dataset S1.

3 Results

3.1 Magma Intrusion Depths in the Main Ethiopian Rift

Our key barometric and geochemical results are presented in Figures 2 and 3, with additional figures presented in the Supporting Information. MIs are entrapped within olivine crystals of composition Fo_{76-88}, and there are no systematic differences in major, trace, or volatile element concentrations between MIs collected from the two cones in this study (Dataset S1). CO_2 concentrations range from 35–5770 ppm in MI glass only; MIs with CO_2 measurements in both the glass and vapor bubble have total combined CO_2 contents of 1895–3248 ppm, with 15–46% of the CO_2 residing within the bubble (Dataset S1). Where an unanalyzed shrinkage bubble is present, CO_2 contents are assumed to be minima and we estimate the plausible range of total CO_2 using our bub-

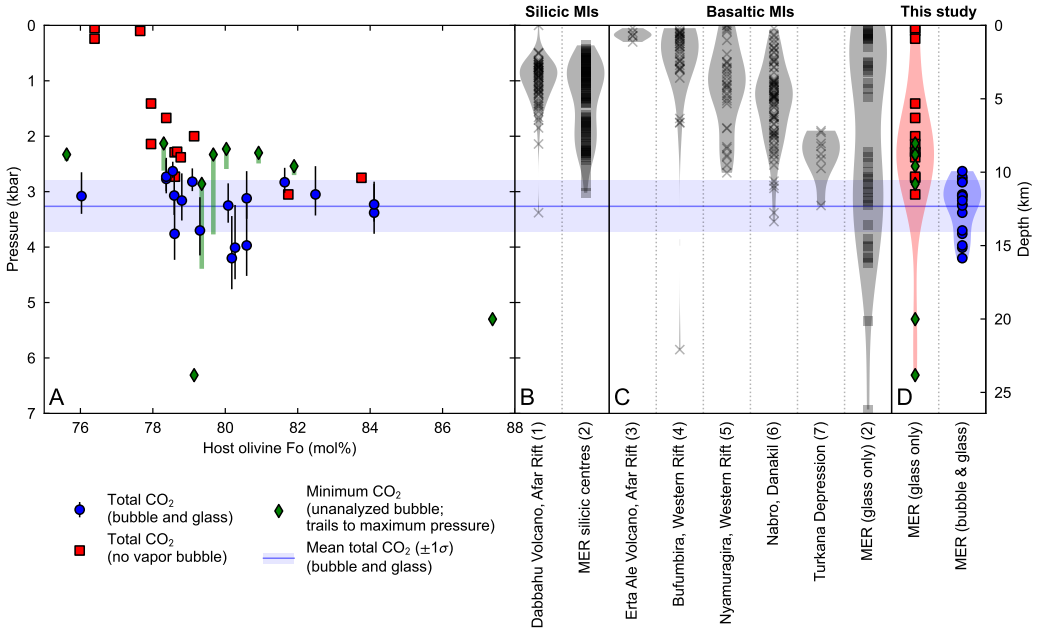

Figure 2. A. Volatile CO_2-H_2O saturation pressures of olivine-hosted MIs from the MER, plotted against MI olivine host Fo (olivine Fo=100·Mg/(Fe+Mg)). MIs are categorized on which components are analyzed. Physical dimensions of MI vapor bubbles that are analyzed only for glass composition can be used to estimate maximum CO_2 if bubble CO_2 density is well characterized (green diamonds); this is performed assuming a density of 0.21 g cm^{-3} (see Supporting Information). Error bars on pressures calculated from MIs for which bubble and glass are analysed are 1σ. B–D. Violin plots of volatile CO_2-H_2O saturation pressures recorded by mineral-hosted MIs from the EARS and Afar calculated using MagmaSat. Saturation pressures are individually determined for each MI using their recorded major and trace element composition and magmatic temperatures. Where FeO_t is provided without Fe_2O_3 all Fe is assumed to be Fe^{2+}. Subfigure B shows distributions of silicic MIs (SiO_2 >60 wt%), subfigure C shows basaltic MIs (SiO_2 <55 wt%), and subfigure D shows the basaltic MIs of this study. The blue line and shaded area across all subfigures marks the mean and 1σ of the MI subset of this study with combined vapor bubble and glass CO_2. References: 1. Field, Blundy, et al. (2012); 2. Iddon and Edmonds (2020), shown as squares for emphasis; 3. Field, Barnie, et al. (2012); 4. Hudgins et al. (2015); 5. Head et al. (2011); 6. A. Donovan et al. (2017); 7. Rooney et al. (2022), without bubble corrections.

ble CO_2 density measurements (see Supporting Information). H_2O concentrations display less variability: discounting the three MIs that have clearly degassed (containing $\leq$0.4 wt% H_2O), MIs have a mean H_2O concentration of 1.1$\pm$0.2 wt% (Supporting Figure S6), which is comparable to H_2O concentrations obtained from other MER and EARS MIs (Iddon & Edmonds, 2020; Rooney et al., 2022).

Volatile saturation pressures of MIs are calculated using the fully thermodynamic MagmaSat volatile solubility model (Ghiorso & Gualda, 2015) via the Python 3 library VESIcal (Iacovino et al., 2021; Wieser et al., 2022); other volatile solubility models are considered and compared in the Supporting Information. Storage pressures for MIs for which total CO_2 contents are known (vapor bubble and glass), determined at a magmatic temperature of 1200 °C (Iddon et al., 2019; Wong et al., 2022), vary over a relatively narrow range from 2.5–4.5 kbar (Figure 2A). In the MER these pressures correspond to depths of ~10–15 km (assuming a crustal density of 2.7 g cm^{-3}), among the deepest recorded volatile saturation depths for continental rift magmas (Figure 2B-D). Pressures recorded by MIs without bubbles overlap partially with those that do have analyzed bubbles; however, the average CO_2 concentration and therefore pressure of MIs without a bubble is typically lower than those with a bubble. Two MIs for which only inclusion glass CO_2 is known record higher pressures in excess of 5 kbar (~20 km), corresponding to the MER lower crust. Overall, our barometric results show a relatively limited distribution of magma storage depths with a narrowly focused zone of intrusion centered at ~12 km depth, coincident with the seismically imaged boundary between the upper and lower crust in the MER (Maguire et al., 2006), and in close agreement with MI volatile saturation pressures from the Turkana Depression to the south of the MER (Figure 2C; Rooney et al., 2022).

3.2 Melt Inclusion Trace Element Compositions

The major element compositions of MIs overlap with carrier basalt (Supporting Figure S8) and whole-rock compositions of erupted lavas (Dataset S1; Tadesse et al., 2019; Nicotra et al., 2021). Incompatible trace element concentrations vary considerably in both MIs and lavas, but nonetheless still overlap (Figures 3A and B). Greater primary compositional variability is preserved in the MIs over the whole rocks, further evidenced by variations in trace element ratios that are not significantly affected by crystal fractionation, e.g., La/Yb and Dy/Yb (Figures 3C and D). While absolute trace element compositions can be achieved by melt fractionation from our most primitive MIs (Figures 3A and B), the scatter in trace element ratios cannot be replicated solely by fractionation of a common parental melt (Figures 3C and D).

By comparing CO_2 concentrations with trace elements with similar behavior during mantle melting (e.g., Ba, Rb), CO_2 degassing from mantle melts can be assessed (e.g., Le Voyer et al., 2018). While primary magmatic CO_2 contents are not known for MER magmas, the highest observed CO_2/Ba and CO_2/Rb ratios approach those measured in undegassed MORB (Le Voyer et al., 2018). Assuming that initial CO_2-trace element ratios are similar to those of MORB, CO_2/Ba and CO_2/Rb systematics for MER MIs clearly show evidence for degassing of CO_2 even in MIs with total CO_2 determinations (Figure 3E). Most melts therefore appear to have lost substantial volumes of CO_2 prior to MI entrapment (Figure 3E). If MORB ratios are reflective of primary CO_2/Ba and CO_2/Rb values in MER melts then initial CO_2 contents will be in the range of 1–4 wt% (mean of 2.0$\pm$0.6 wt% with the same CO_2/Ba as MORB), with ~60–95% of the CO_2 having been exsolved at mid-crustal pressures.

CO_2 degassing in the MER, likely derived from degassing of intruded mid-crustal magmas, is focused along discrete fault zones (Hunt et al., 2017). By making assumptions on the volumes of melt intruded into the crust (e.g., Iddon & Edmonds, 2020), we determine that the difference between expected CO_2 concentrations in primary mantle

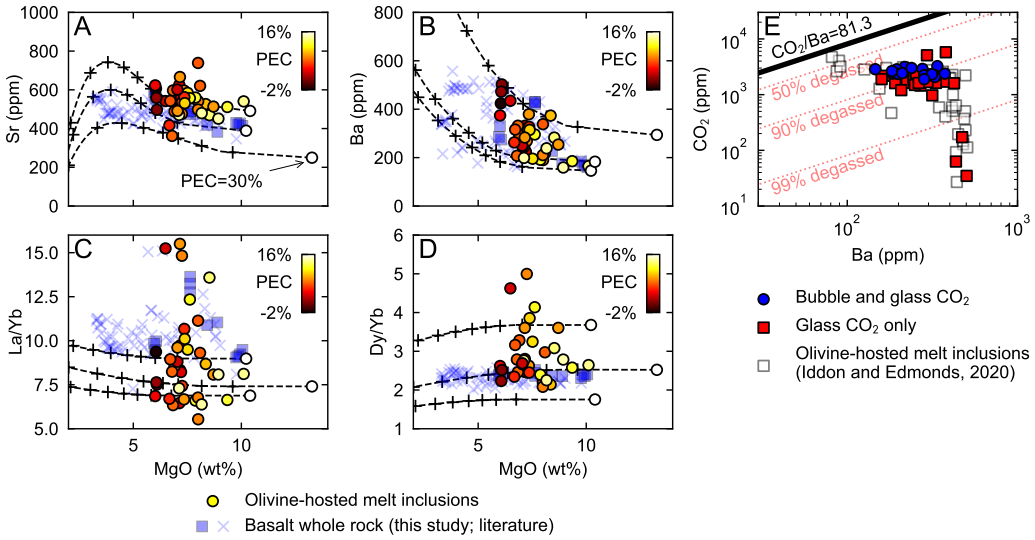

Figure 3. A–D. MI and whole-rock trace element and trace element ratios plotted against MgO (this study; Tadesse et al., 2019; Nicotra et al., 2021). Liquid lines of descent with crosses denoting 10% fractionation intervals are determined from our three highest MgO melts using Rhyolite-MELTS v1.2.0 (Gualda et al., 2012, see Supporting Information), assuming Rayleigh fractionation with the partition coefficients collated by Iddon and Edmonds (2020). PEC corrections are detailed in the Supporting Information. E. Olivine-hosted MI CO_2 plotted against Ba; primary CO_2/Ba of MORB (Le Voyer et al., 2018).

melts and those observed in our MIs is sufficient to generate the CO_2 fluxes measured from surface degassing (Figure 3E Hunt et al., 2017, see Supporting Information). The restriction of significant degassing to localized regions in the MER (Hunt et al., 2017) may suggest that some regions are subject to active intrusion at the present day whereas other portions are not; future studies should aim to constrain this periodicity of melt emplacement.

4 Discussion

4.1 Depths of Intrusion in the East African Rift

Our total CO_2 saturation pressures determined from vapor bubble and glass are in broad agreement with maximum pressures of melt storage estimated from MI volatiles at other EARS sectors (Figure 2B–D). Applying the same volatile solubility modelling performed on our MIs to literature datasets, we determine that our proposed 10–15 km depth range for basalt storage coincides with the deepest MIs at other parts of the EARS and Afar Rift (Figure 2C; e.g., A. Donovan et al., 2017; Rooney et al., 2022). Geophysical observations of crustal melt movement in other sectors of the EARS (Weinstein et al., 2017; Reiss et al., 2021, 2022) suggests that melt focusing at these pressures may be ubiquitous within the EARS.

The lack of evidence for significant melt storage within the upper crust in our dataset contrasts with the depth distributions for magma storage obtained from suites of MIs collected at large caldera-forming volcanic centers found along the MER (Figure 2; Iddon & Edmonds, 2020). Under these silicic centers, melt storage appears to extend upwards into the upper crust, where evolved magmas are generated via low pressure frac-

tionation (Iddon & Edmonds, 2020). Notably, the maximum storage depths under caldera complexes in the EARS identified both from MI volatile saturation barometry (Figure 2; Iddon & Edmonds, 2020; Rooney et al., 2022) and from mineral barometry (Rooney et al., 2005; Iddon et al., 2019) coincides with the 10–15 km depth range observed in our dataset. This depth range may therefore be the locus of initial basaltic melt emplacement along the MER, with important implications for heat distribution within the rifting crust and therefore crustal strength profiles (Buck, 2006; Daniels et al., 2014; Lavecchia et al., 2016), such as the creation of a mid-crustal weak layer (Muluneh et al., 2020). With the exception of those below caldera complexes/silicic volcanoes (e.g., Biggs et al., 2011), upper crustal melt bodies (<10 km depth) in the MER are likely to be ephemeral, perhaps forming during periodic intrusive-eruptive episodes (e.g., Ebinger et al., 2013).

In contrast to the extensive MI data corresponding to mid-crustal pressures, very few MIs from our dataset and the MER dataset of Iddon and Edmonds (2020) record pressures corresponding to the lower crust or Moho (Figure 2; e.g., Maguire et al., 2006; Lavayssière et al., 2018). Considering the evolved compositions of our olivines (mean Fo_{80}) relative to Fo_{90} olivines in other MER volcanic materials (e.g., Rooney et al., 2005), we posit that an initial stage of fractionation near the Moho prior to ascent to mid-crustal pressures is necessary. This hypothesis is supported by low wavespeeds observed at Moho depths from the presence of melt in the heavily intruded lower crust (Keranen et al., 2009; Chambers et al., 2019, 2021), and numerical models suggesting that the lowermost crust is weak, hot and underlies a lower-crustal brittle-ductile transition at 20–25 km (Lavecchia et al., 2016; Muluneh et al., 2020). The absence of strong radial seismic anisotropy in the lower crust may also imply that melt storage at these depths may comprise both sills and isotropic bodies (Chambers et al., 2021). Melts pooling and fractionating at the base of the crust may bypass the ductile lowermost crust entirely if both density differences between melt and crust and lower crustal strain rates are sufficiently high (Muluneh et al., 2021).

4.2 Compositional Heterogeneity in Melt Inclusions

Variability in absolute trace element concentrations (Figures 3A and B) could result from fractional crystallization of distinct parental melts and/or mixing between variably fractionated melts with distinct origins. In contrast, the broader distribution of trace element ratios observed in MIs relative to whole rocks (Figures 3C and D) can only be inherited from the compositional heterogeneity of parental mantle-derived melts. Such variability may be derived from the melting of multiple source lithologies (e.g., Shorttle & Maclennan, 2011) and/or unmixed fractional mantle melts (e.g., Gurenko & Chaussidon, 1995).

Physical interactions between intrusive bodies therefore appear to be limited, and we infer that intruded magmas reside in a series of discrete sills emplaced at a common depth. The slightly lower degree of compositional diversity observed in erupted lavas (Figures 3C and D), even at higher MgO, suggests that some mixing does occur prior to eruption and that dyke intrusion into the upper crust may involve partially homogenized melts sourced from multiple mid-crustal sills. Erupted melts extend to lower MgO than the MIs (after PEC corrections), and pre-eruptive mixing and homogenization may therefore occur during a final stage of differentiation within upper crustal magma bodies.

4.3 Basaltic Melt Focusing in the Main Ethiopian Rift

The presence of melts intruded as mid-crustal sill complexes is strongly supported by geophysical observations of the present-day MER crust. Strong horizontally oriented seismic anisotropy observed in the MER at depths of 10–15 km is consistent with the presence of sills (Chambers et al., 2021). Low seismic moment earthquakes in northern MER magmatic segments are distributed within a narrow depth band between 8–16 km

and have been interpreted as being triggered by movement or emplacement of mid-crustal melts (Keir et al., 2006; Daly et al., 2008). High Vp, high-Vp/Vs and high-density bodies are inferred to be present at these depths under Boku and other MER segments (Keranen et al., 2004; Cornwell et al., 2006; Daly et al., 2008), as are high-conductivity crustal anomalies (Whaler & Hautot, 2006), all indicative of partially molten intrusions in the mid-crust. Our results are also in good agreement with empirical observations relating MER cone clustering to melt intrusion depths (Mazzarini et al., 2013). In other words, the melt storage depths resolved directly using petrological methods are in very close agreement with the deepest intrusion pressures determined using geophysical techniques.

Focusing of ascending basaltic melts at this depth range can, to a first order, be attributed to MER crustal density structure as the mean density of the lower crust exceeds that of our MIs (mean of 2.71 g cm^{-3}, calculated after PEC corrections using DensityX, Iacovino and Till (2019); cf. e.g., Cornwell et al. (2006)). Driven by density differences, basaltic melts will rise to mid-crustal depths before they achieve neutral buoyancy, stall and crystallize. The upper crust, comparatively less dense than the lower crust, will limit the ascent of basalt melts beyond the focusing zone (Cornwell et al., 2006; Mickus et al., 2007).

Melt focusing in the mid-crust could also be attributed to the rheological structure of the crust. Numerical models based on seismic observations suggest that the 10–15 km depth range resolved using our MIs coincides with the weakest part of the Ethiopian crust, which is sandwiched between two strong brittle layers in the upper and mid-lower crust (Muluneh et al., 2020). The strong, lower-density brittle crust above this ductile zone, combined with the density limitations discussed above, likely inhibits further ascent of the buoyant melt (Cornwell et al., 2006; Muluneh et al., 2020). Melt may only progress directly to the surface through the breaking of dyke-induced faults (e.g., Casey et al., 2006), by exploiting pre-existing crustal weaknesses (e.g., Le Corvec et al., 2013), or after extensive fractionation to form lower-density silicic melts (e.g., Gleeson et al., 2017).

We therefore hypothesise that the intrusion and emplacement of melts into this weak, ductile mid-crust will have a strong effect on the overall rheology of the rifting crust, which in turn may govern how the crust locally accommodates strain in response to far-field extensional stresses. Ductile stretching may accommodate crustal deformation at a different rate or manner relative to the brittle layers above and below this weak zone, in turn possibly dictating that future batches of melt are focused in the same region. Indeed, the development of crustal sill systems in the MER may arise from pulsed emplacement of magmas from the lower crust or mantle (e.g., Annen et al., 2015). Stacked sills formed in this manner may maintain high localized temperatures in the crust, which can facilitate further intrusion of melt at shallower pressures, or may themselves contract during cooling to generate accommodation space for further intrusions (Magee et al., 2016). Future numerical or analog models of rift deformation in Ethiopia must account for the development of a hot, ductile, weak layer in the crust, and the influences such a layer may have on overall crustal rheology.

5 Summary

The results of our study are summarized in Figure 4. Through the careful analysis of major, trace, and volatile elements in olivine-hosted MIs, we propose that stacked mid-crustal sills in the depth range of 10–15 km are the dominant form of magmatic storage in the MER (Figures 4A and B). These sills are known to be horizontally oriented from seismic anisotropy (Chambers et al., 2019), and develop as a consequence of repeated magmatic intrusion into the mid-crust during the progression of late-stage continental rifting. Initially crystallizing at or near the Moho, mantle-derived magmas bypass the ductile lowermost crust to arrive at the Ethiopian mid-crust, heralded by seismic activity during emplacement (Figure 4C). These melts are stored as discrete sills in the weak,

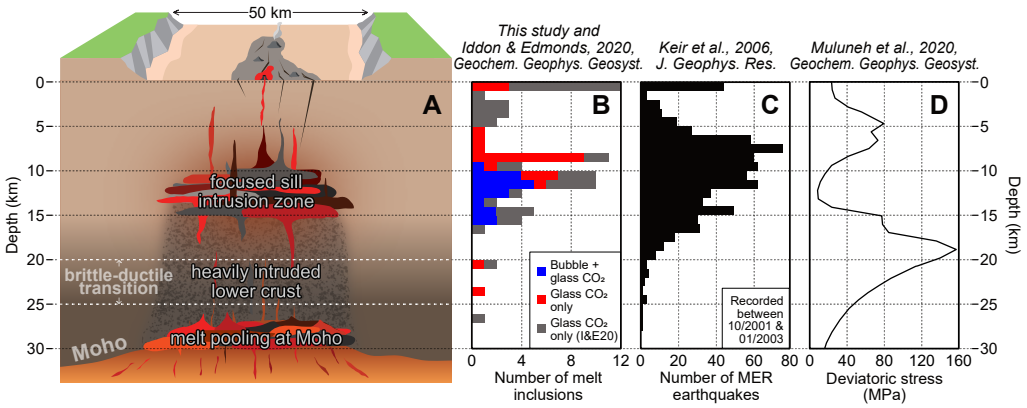

Figure 4. A. Summary cartoon illustrating our proposed structure of the MER crust. Horizontal and vertical dimensions not to same scale. B. Histogram of MER olivine-hosted MI saturation pressures (this study; Iddon & Edmonds, 2020). C. Histogram of MER earthquakes recorded between October 2001 and January 2003 (Keir et al., 2006; Daly et al., 2008, selection criteria in Supporting Figure S9). D. Numerical model of MER crustal deviatoric stress (Muluneh et al., 2020).

ductile mid-crust and blocked from further ascent by a strong, lower density upper crust (Figure 4D). The diverse range of trace element ratios observed in MIs gives evidence to limited melt mixing in the crust; partial mixing of magmas between sills may occur in the shallow crust prior to eruption (Figure 3). Petrological evidence for mid-crustal sills in the MER presented in this study is in agreement with geophysical observations (e.g., Keranen et al., 2004), and the volatile composition of basalts comprising these bodies are consistent with CO_2 degassing rates measured at the rift floor (Hunt et al., 2017). The presence of hot sills in the MER mid-crust has important implications for how intruding melts in late-stage rifts affect and are affected by the rheological structure of the crust, and should be considered a key element in future development of models of continental rifting.

6 Open Research

The complete dataset of geochemical analyses and melt inclusion microscope photographs is available within a Zenodo repository (`doi.org/10.5281/zenodo.7236254`).

Acknowledgments

KW and PW are funded by NERC DTP studentships NE/L002574/1 and NE/L002507/1 respectively. KW acknowledges additional financial support from the Geologists' Association New Researchers Award. Ion probe analyses are funded through NERC grant IMF694/1119 awarded to DF. ME acknowledges the support of COMET via NERC. We thank Cristina Talavera Rodriguez and Lesley Neve for performing geochemical analyses on our behalf during the COVID-19 pandemic. Yared Sinetebeb, Harri Wyn Williams, Emilie Ringe, and Richard Walshaw are thanked for assistance with fieldwork, sample preparation, Raman spectroscopy, and EPMA respectively. We acknowledge thought-provoking discussions with Ian Bastow, Emma Chambers, Tim Craig, Sophie Hautot, Derek Keir, Tyrone Rooney, and Kathy Whaler. Finally, we acknowledge the Ethiopian Ministry of Mines and Oromia State Administration for sampling and field permissions.

References

Allison, C. M., Roggensack, K., & Clarke, A. B. (2019, June). H_2O–CO_2 solubility in alkali-rich mafic magmas: new experiments at mid-crustal pressures. *Contributions to Mineralogy and Petrology*, *174*(7), 58. Retrieved 2022-02-01, from https://doi.org/10.1007/s00410-019-1592-4 doi: 10.1007/s00410-019-1592-4

Annen, C., Blundy, J. D., Leuthold, J., & Sparks, R. S. J. (2015, August). Construction and evolution of igneous bodies: Towards an integrated perspective of crustal magmatism. *Lithos*, *230*, 206–221. Retrieved 2022-12-09, from https://www.sciencedirect.com/science/article/pii/S0024493715001759 doi: 10.1016/j.lithos.2015.05.008

Armitage, J. J., Ferguson, D. J., Goes, S., Hammond, J. O. S., Calais, E., Rychert, C. A., & Harmon, N. (2015, May). Upper mantle temperature and the onset of extension and break-up in Afar, Africa. *Earth and Planetary Science Letters*, *418*, 78–90. Retrieved 2018-10-03, from http://www.sciencedirect.com/science/article/pii/S0012821X15001259 doi: 10.1016/j.epsl.2015.02.039

Bastow, I. D., & Keir, D. (2011, April). The protracted development of the continent–ocean transition in Afar. *Nature Geoscience*, *4*(4), 248–250. Retrieved 2018-05-16, from https://www.nature.com/articles/ngeo1095 doi: 10.1038/ngeo1095

Bastow, I. D., Keir, D., & Daly, E. (2011, June). The Ethiopia Afar Geoscientific Lithospheric Experiment (EAGLE): Probing the transition from continental rifting to incipient seafloor spreading. In *Geological Society of America Special Papers* (Vol. 478, pp. 51–76). Geological Society of America. Retrieved 2018-10-26, from https://pubs.geoscienceworld.org/books/book/653/chapter/3806991/ doi: 10.1130/2011.2478(04)

Bastow, I. D., Pilidou, S., Kendall, J.-M., & Stuart, G. W. (2010, June). Melt-induced seismic anisotropy and magma assisted rifting in Ethiopia: Evidence from surface waves. *Geochemistry, Geophysics, Geosystems*, *11*(6). Retrieved 2018-11-02, from https://agupubs.onlinelibrary.wiley.com/doi/full/10.1029/2010GC003036 doi: 10.1029/2010GC003036

Bialas, R. W., Buck, W. R., & Qin, R. (2010, March). How much magma is required to rift a continent? *Earth and Planetary Science Letters*, *292*(1), 68–78. Retrieved 2022-11-29, from https://www.sciencedirect.com/science/article/pii/S0012821X10000555 doi: 10.1016/j.epsl.2010.01.021

Biggs, J., Bastow, I. D., Keir, D., & Lewi, E. (2011, September). Pulses of deformation reveal frequently recurring shallow magmatic activity beneath the Main Ethiopian Rift. *Geochemistry, Geophysics, Geosystems*, *12*(9). Retrieved 2019-02-05, from https://agupubs.onlinelibrary.wiley.com/doi/full/10.1029/2011GC003662 doi: 10.1029/2011GC003662

Blundy, J. D., & Wood, B. J. (1991, January). Crystal-chemical controls on the partitioning of Sr and Ba between plagioclase feldspar, silicate melts, and hydrothermal solutions. *Geochimica et Cosmochimica Acta*, *55*(1), 193–209. Retrieved 2017-05-25, from http://www.sciencedirect.com/science/article/pii/001670379190411W doi: 10.1016/0016-7037(91)90411-W

Buck, W. R. (2006, January). The role of magma in the development of the Afro-Arabian Rift System. In G. Yirgu, C. Ebinger, & P. K. H. Maguire (Eds.), *The Afar Volcanic Province within the East African Rift System* (Vol. 259, pp. 43–54). Retrieved 2018-11-05, from http://sp.lyellcollection.org/content/259/1/43

Casey, M., Ebinger, C., Keir, D., Gloaguen, R., & Mohamed, F. (2006, January). Strain accommodation in transitional rifts: extension by magma intrusion and faulting in Ethiopian rift magmatic segments. In G. Yirgu, C. J. Ebinger, & P. K. H. Maguire (Eds.), *The Afar Volcanic Province within the East African Rift System* (Vol. 259, pp. 143–163). Retrieved 2018-09-23, from

http://sp.lyellcollection.org/content/259/1/143

Chambers, E. L., Harmon, N., Keir, D., & Rychert, C. A. (2019, April). Using Ambient Noise to Image the Northern East African Rift. *Geochemistry, Geophysics, Geosystems*, *20*(4), 2091–2109. Retrieved 2019-06-21, from https://agupubs.onlinelibrary.wiley.com/doi/full/10.1029/2018GC008129 doi: 10.1029/2018GC008129

Chambers, E. L., Harmon, N., Rychert, C. A., & Keir, D. (2021, November). Variations in melt emplacement beneath the northern East African Rift from radial anisotropy. *Earth and Planetary Science Letters*, *573*, 117150. Retrieved 2021-11-03, from https://linkinghub.elsevier.com/retrieve/pii/S0012821X21004052 doi: 10.1016/j.epsl.2021.117150

Cornwell, D. G., Mackenzie, G. D., England, R. W., Maguire, P. K. H., Asfaw, L. M., & Oluma, B. (2006, January). Northern Main Ethiopian Rift crustal structure from new high-precision gravity data. In *The Afar Volcanic Province within the East African Rift System* (Vol. 259, pp. 307–321). Retrieved 2018-11-14, from http://sp.lyellcollection.org/content/259/1/307

Daly, E., Keir, D., Ebinger, C. J., Stuart, G. W., Bastow, I. D., & Ayele, A. (2008, March). Crustal tomographic imaging of a transitional continental rift: The Ethiopian rift. *Geophysical Journal International*, *172*(3), 1033–1048. Retrieved 2018-11-01, from https://academic.oup.com/gji/article/172/3/1033/571185 doi: 10.1111/j.1365-246X.2007.03682.x

Daniels, K. A., Bastow, I. D., Keir, D., Sparks, R. S. J., & Menand, T. (2014, January). Thermal models of dyke intrusion during development of continent–ocean transition. *Earth and Planetary Science Letters*, *385*, 145–153. Retrieved 2018-11-22, from http://www.sciencedirect.com/science/article/pii/S0012821X13005293 doi: 10.1016/j.epsl.2013.09.018

Danyushevsky, L. V. (2001, October). The effect of small amounts of H_2O on crystallisation of mid-ocean ridge and backarc basin magmas. *Journal of Volcanology and Geothermal Research*, *110*(3), 265–280. Retrieved 2021-03-30, from https://www.sciencedirect.com/science/article/pii/S037702730100213X doi: 10.1016/S0377-0273(01)00213-X

Danyushevsky, L. V., & Plechov, P. (2011, July). Petrolog3: Integrated software for modeling crystallization processes. *Geochemistry, Geophysics, Geosystems*, *12*(7), Q07021. Retrieved 2017-12-02, from http://onlinelibrary.wiley.com/doi/10.1029/2011GC003516/abstract doi: 10.1029/2011GC003516

DeVitre, C. L., Barth, A., Gazel, E., Plank, T. A., & Ramalho, R. (2021, December). Solving the Carbonate Problem in Melt Inclusion Bubbles. In *AGU Fall Meeting Abstracts.* Retrieved from https://agu.confex.com/agu/fm21/meetingapp.cgi/Paper/845682

DeVitre, C. L., Dayton, K., Gazel, E., Barth, A., Plank, T. A., Pamukcu, A., ... Monteleone, B. (2022, July). Accounting for Multi-Phase Carbon in Melt Inclusion Bubbles. In *Goldschmidt Conference Abstracts.* Retrieved 2022-08-08, from https://conf.goldschmidt.info/goldschmidt/2022/meetingapp.cgi/Paper/12601

Dixon, J. E. (1997, April). Degassing of alkalic basalts. *American Mineralogist*, *82*(3-4), 368–378. Retrieved 2022-01-05, from https://pubs.geoscienceworld.org/ammin/article/82/3-4/368-378/43291 doi: 10.2138/am-1997-3-415

Dixon, J. E., Stolper, E. M., & Holloway, J. R. (1995, December). An Experimental Study of Water and Carbon Dioxide Solubilities in Mid-Ocean Ridge Basaltic Liquids. Part I: Calibration and Solubility Models. *Journal of Petrology*, *36*(6), 1607–1631. Retrieved 2019-04-08, from https://academic.oup.com/petrology/article/36/6/1607/1493308 doi: 10.1093/oxfordjournals.petrology.a037267

Donovan, A., Blundy, J., Oppenheimer, C., & Buisman, I. (2017, November). The

2011 eruption of Nabro volcano, Eritrea: perspectives on magmatic processes from melt inclusions. *Contributions to Mineralogy and Petrology*, *173*(1), 1. Retrieved 2022-01-17, from https://doi.org/10.1007/s00410-017-1425-2 doi: 10.1007/s00410-017-1425-2

Donovan, J. J. (2021). *Probe for EPMA v. 13.0.5 User's Guide and Reference (Xtreme Edition).* Retrieved 2022-06-07, from https://probesoftware.com/download/PROBEWIN.pdf

Ebinger, C. J., Keir, D., Ayele, A., Calais, E., Wright, T. J., Belachew, M., ... Buck, W. R. (2008, September). Capturing magma intrusion and faulting processes during continental rupture: Seismicity of the Dabbahu (Afar) rift. *Geophysical Journal International*, *174*(3), 1138–1152. Retrieved 2021-02-01, from https://doi.org/10.1111/j.1365-246X.2008.03877.x doi: 10.1111/j.1365-246X.2008.03877.x

Ebinger, C. J., van Wijk, J., & Keir, D. (2013, September). The time scales of continental rifting: Implications for global processes. In *Geological Society of America Special Papers* (Vol. 500, pp. 371–396). Geological Society of America. Retrieved 2018-05-18, from https://pubs.geoscienceworld.org/books/book/671/chapter/3807783/ doi: 10.1130/2013.2500(11)

Field, L., Barnie, T., Blundy, J., Brooker, R. A., Keir, D., Lewi, E., & Saunders, K. (2012, December). Integrated field, satellite and petrological observations of the November 2010 eruption of Erta Ale. *Bulletin of Volcanology*, *74*(10), 2251–2271. Retrieved 2019-08-21, from https://doi.org/10.1007/s00445-012-0660-7 doi: 10.1007/s00445-012-0660-7

Field, L., Blundy, J., Brooker, R. A., Wright, T., & Yirgu, G. (2012, July). Magma storage conditions beneath Dabbahu Volcano (Ethiopia) constrained by petrology, seismicity and satellite geodesy. *Bulletin of Volcanology*, *74*(5), 981–1004. Retrieved 2019-02-05, from http://link.springer.com/10.1007/s00445-012-0580-6 doi: 10.1007/s00445-012-0580-6

Foley, S. F., & Fischer, T. P. (2017, December). An essential role for continental rifts and lithosphere in the deep carbon cycle. *Nature Geoscience*, *10*(12), 897–902. Retrieved 2018-07-18, from https://www.nature.com/articles/s41561-017-0002-7 doi: 10.1038/s41561-017-0002-7

Ghiorso, M. S., & Gualda, G. A. R. (2015, June). An H_2O–CO_2 mixed fluid saturation model compatible with rhyolite-MELTS. *Contributions to Mineralogy and Petrology*, *169*(6), 53. Retrieved 2021-11-25, from https://doi.org/10.1007/s00410-015-1141-8 doi: 10.1007/s00410-015-1141-8

Gleeson, M. L. M., Stock, M. J., Pyle, D. M., Mather, T. A., Hutchison, W., Yirgu, G., & Wade, J. (2017, May). Constraining magma storage conditions at a restless volcano in the Main Ethiopian Rift using phase equilibria models. *Journal of Volcanology and Geothermal Research*, *337*, 44–61. Retrieved 2018-10-24, from http://www.sciencedirect.com/science/article/pii/S0377027316304383 doi: 10.1016/j.jvolgeores.2017.02.026

Gualda, G. A. R., Ghiorso, M. S., Lemons, R. V., & Carley, T. L. (2012, May). Rhyolite-MELTS: a Modified Calibration of MELTS Optimized for Silica-rich, Fluid-bearing Magmatic Systems. *Journal of Petrology*, *53*(5), 875–890. Retrieved 2021-03-24, from https://doi.org/10.1093/petrology/egr080 doi: 10.1093/petrology/egr080

Gurenko, A. A., & Chaussidon, M. (1995, July). Enriched and depleted primitive melts included in olivine from Icelandic tholeiites: origin by continuous melting of a single mantle column. *Geochimica et Cosmochimica Acta*, *59*(14), 2905–2917. Retrieved 2021-12-09, from https://www.sciencedirect.com/science/article/pii/0016703795001840 doi: 10.1016/0016-7037(95)00184-0

Hartley, M. E., Maclennan, J., Edmonds, M., & Thordarson, T. (2014, May). Reconstructing the deep CO_2 degassing behaviour of large basaltic fissure eruptions. *Earth and Planetary Science Letters*, *393*, 120–131. Retrieved 2018-02-16, from

http://www.sciencedirect.com/science/article/pii/S0012821X14001125 doi: 10.1016/j.epsl.2014.02.031

Hauri, E., Wang, J., Dixon, J. E., King, P. L., Mandeville, C., & Newman, S. (2002, March). SIMS analysis of volatiles in silicate glasses: 1. Calibration, matrix effects and comparisons with FTIR. *Chemical Geology*, *183*(1), 99–114. Retrieved 2022-02-21, from https://www.sciencedirect.com/science/article/pii/S0009254101003758 doi: 10.1016/S0009-2541(01)00375-8

Head, E. M., Shaw, A. M., Wallace, P. J., Sims, K. W. W., & Carn, S. A. (2011). Insight into volatile behavior at Nyamuragira volcano (D.R. Congo, Africa) through olivine-hosted melt inclusions. *Geochemistry, Geophysics, Geosystems*, *12*(10). Retrieved 2022-01-17, from https://onlinelibrary.wiley.com/doi/abs/10.1029/2011GC003699 (_eprint: https://onlinelibrary.wiley.com/doi/pdf/10.1029/2011GC003699) doi: 10.1029/2011GC003699

Hudgins, T. R., Mukasa, S. B., Simon, A. C., Moore, G., & Barifaijo, E. (2015, April). Melt inclusion evidence for CO_2-rich melts beneath the western branch of the East African Rift: implications for long-term storage of volatiles in the deep lithospheric mantle. *Contributions to Mineralogy and Petrology*, *169*(5), 46. Retrieved 2020-09-15, from https://doi.org/10.1007/s00410-015-1140-9 doi: 10.1007/s00410-015-1140-9

Hunt, J. A., Zafu, A., Mather, T. A., Pyle, D. M., & Barry, P. H. (2017, October). Spatially Variable CO_2 Degassing in the Main Ethiopian Rift: Implications for Magma Storage, Volatile Transport, and Rift-Related Emissions. *Geochemistry, Geophysics, Geosystems*, *18*(10), 3714–3737. Retrieved 2018-08-07, from https://agupubs.onlinelibrary.wiley.com/doi/abs/10.1002/2017GC006975 doi: 10.1002/2017GC006975

Iacono-Marziano, G., Morizet, Y., Le Trong, E., & Gaillard, F. (2012, November). New experimental data and semi-empirical parameterization of H_2O–CO_2 solubility in mafic melts. *Geochimica et Cosmochimica Acta*, *97*, 1–23. Retrieved 2020-02-17, from http://www.sciencedirect.com/science/article/pii/S0016703712004930 doi: 10.1016/j.gca.2012.08.035

Iacovino, K., Matthews, S., Wieser, P. E., Moore, G. M., & Bégué, F. (2021). VESIcal Part I: An Open-Source Thermodynamic Model Engine for Mixed Volatile (H_2O-CO_2) Solubility in Silicate Melts. *Earth and Space Science*, *8*(11), e2020EA001584. Retrieved 2021-11-16, from https://onlinelibrary.wiley.com/doi/abs/10.1029/2020EA001584 (_eprint: https://onlinelibrary.wiley.com/doi/pdf/10.1029/2020EA001584) doi: 10.1029/2020EA001584

Iacovino, K., & Till, C. B. (2019, February). DensityX: A program for calculating the densities of magmatic liquids up to 1,627 °C and 30 kbar. *Volcanica*, *2*(1), 1–10. Retrieved 2021-03-04, from http://jvolcanica.org/ojs/index.php/volcanica/article/view/12 (Number: 1) doi: 10.30909/vol.02.01.0110

Iddon, F., & Edmonds, M. (2020). Volatile-Rich Magmas Distributed Through the Upper Crust in the Main Ethiopian Rift. *Geochemistry, Geophysics, Geosystems*, *21*(6), e2019–GC008904. Retrieved 2020-06-24, from https://agupubs.onlinelibrary.wiley.com/doi/abs/10.1029/2019GC008904 (_eprint: https://agupubs.onlinelibrary.wiley.com/doi/pdf/10.1029/2019GC008904) doi: 10.1029/2019GC008904

Iddon, F., Jackson, C., Hutchison, W., Fontijn, K., Pyle, D. M., Mather, T. A., ... Edmonds, M. (2019). Mixing and Crystal Scavenging in the Main Ethiopian Rift Revealed by Trace Element Systematics in Feldspars and Glasses. *Geochemistry, Geophysics, Geosystems*, *20*(1), 230–259. Retrieved 2019-10-02, from https://agupubs.onlinelibrary.wiley.com/doi/abs/10.1029/2018GC007836 doi: 10.1029/2018GC007836

Jarosewich, E. (2002). Smithsonian Microbeam Standards. *Journal of Research*

of the National Institute of Standards and Technology, *107*(6), 681–685. Retrieved 2022-02-21, from https://www.ncbi.nlm.nih.gov/pmc/articles/PMC4863845/ doi: 10.6028/jres.107.054

Jochum, K. P., Stoll, B., Herwig, K., Willbold, M., Hofmann, A. W., Amini, M., ... Woodhead, J. D. (2006). MPI-DING reference glasses for in situ microanalysis: New reference values for element concentrations and isotope ratios. *Geochemistry, Geophysics, Geosystems*, *7*(2). Retrieved 2021-06-15, from https://agupubs.onlinelibrary.wiley.com/doi/abs/10.1029/2005GC001060 (_eprint: https://agupubs.onlinelibrary.wiley.com/doi/pdf/10.1029/2005GC001060) doi: 10.1029/2005GC001060

Keir, D., Ebinger, C. J., Stuart, G. W., Daly, E., & Ayele, A. (2006, May). Strain accommodation by magmatism and faulting as rifting proceeds to breakup: Seismicity of the northern Ethiopian rift. *Journal of Geophysical Research: Solid Earth*, *111*(B5). Retrieved 2018-11-01, from https://agupubs.onlinelibrary.wiley.com/doi/full/10.1029/2005JB003748 doi: 10.1029/2005JB003748

Kendall, J.-M., Stuart, G. W., Ebinger, C. J., Bastow, I. D., & Keir, D. (2005, January). Magma-assisted rifting in Ethiopia. *Nature*, *433*(7022), 146–148. Retrieved 2018-04-11, from https://www.nature.com/articles/nature03161 doi: 10.1038/nature03161

Keranen, K. M., Klemperer, S. L., Gloaguen, R., & EAGLE Working Group. (2004). Three-dimensional seismic imaging of a protoridge axis in the Main Ethiopian rift. *Geology*, *32*(11), 949. Retrieved 2018-11-01, from https://pubs.geoscienceworld.org/geology/article/32/11/949-952/103645 doi: 10.1130/G20737.1

Keranen, K. M., Klemperer, S. L., Julia, J., Lawrence, J. F., & Nyblade, A. A. (2009, May). Low lower crustal velocity across Ethiopia: Is the Main Ethiopian Rift a narrow rift in a hot craton? *Geochemistry, Geophysics, Geosystems*, *10*(5). Retrieved 2018-11-05, from https://agupubs.onlinelibrary.wiley.com/doi/abs/10.1029/2008GC002293 doi: 10.1029/2008GC002293

Lamadrid, H., Moore, L., Moncada, D., Rimstidt, J., Burruss, R., & Bodnar, R. (2017, February). Reassessment of the Raman CO_2 densimeter. *Chemical Geology*, *450*, 210–222. Retrieved 2020-02-09, from https://linkinghub.elsevier.com/retrieve/pii/S0009254116306945 doi: 10.1016/j.chemgeo.2016.12.034

Lavayssière, A., Rychert, C., Harmon, N., Keir, D., Hammond, J. O. S., Kendall, J.-M., ... Leroy, S. (2018, October). Imaging Lithospheric Discontinuities Beneath the Northern East African Rift Using S-to-P Receiver Functions. *Geochemistry, Geophysics, Geosystems*. Retrieved 2018-11-19, from https://agupubs.onlinelibrary.wiley.com/doi/abs/10.1029/2018GC007463 doi: 10.1029/2018GC007463

Lavecchia, A., Beekman, F., Clark, S. R., & Cloetingh, S. A. P. L. (2016, August). Thermo-rheological aspects of crustal evolution during continental breakup and melt intrusion: The Main Ethiopian Rift, East Africa. *Tectonophysics*, *686*, 51–62. Retrieved 2022-06-01, from https://www.sciencedirect.com/science/article/pii/S0040195116302840 doi: 10.1016/j.tecto.2016.07.018

Le Corvec, N., Menand, T., & Lindsay, J. (2013). Interaction of ascending magma with pre-existing crustal fractures in monogenetic basaltic volcanism: an experimental approach. *Journal of Geophysical Research: Solid Earth*, *118*(3), 968–984. Retrieved 2022-11-25, from https://onlinelibrary.wiley.com/doi/abs/10.1002/jgrb.50142 (_eprint: https://onlinelibrary.wiley.com/doi/pdf/10.1002/jgrb.50142) doi: 10.1002/jgrb.50142

Lee, H., Muirhead, J. D., Fischer, T. P., Ebinger, C. J., Kattenhorn, S. A., Sharp,

Z. D., & Kianji, G. (2016, February). Massive and prolonged deep carbon emissions associated with continental rifting. *Nature Geoscience*, *9*(2), 145–149. Retrieved 2018-07-25, from https://www.nature.com/articles/ngeo2622 doi: 10.1038/ngeo2622

Le Voyer, M., Hauri, E. H., Cottrell, E., Kelley, K. A., Salters, V. J. M., Langmuir, C. H., ... Füri, E. (2018). Carbon fluxes and primary magma CO_2 contents along the global mid-ocean ridge system. *Geochemistry, Geophysics, Geosystems*, *20*(3), 1387–1424. Retrieved 2018-12-03, from https://agupubs.onlinelibrary.wiley.com/doi/abs/10.1029/2018GC007630 doi: 10.1029/2018GC007630

Maclennan, J. (2017, February). Bubble formation and decrepitation control the CO_2 content of olivine-hosted melt inclusions. *Geochemistry, Geophysics, Geosystems*, *18*(2), 597–616. Retrieved 2018-11-14, from https://agupubs.onlinelibrary.wiley.com/doi/abs/10.1002/2016GC006633 doi: 10.1002/2016GC006633

Magee, C., Muirhead, J. D., Karvelas, A., Holford, S. P., Jackson, C. A., Bastow, I. D., ... Shtukert, O. (2016, June). Lateral magma flow in mafic sill complexes. *Geosphere*, *12*(3), 809–841. Retrieved 2022-05-09, from https://doi.org/10.1130/GES01256.1 doi: 10.1130/GES01256.1

Maguire, P., Keller, G., Klemperer, S., Mackenzie, G., Keranen, K., Harder, S., ... Amha, M. (2006). Crustal structure of the northern Main Ethiopian Rift from the EAGLE controlled-source survey; a snapshot of incipient lithospheric break-up. In *The Afar Volcanic Province within the East African Rift System* (Vol. 259, pp. 269–292). Retrieved 2018-11-26, from http://sp.lyellcollection.org/lookup/doi/10.1144/GSL.SP.2006.259.01.21

Mazzarini, F., Rooney, T. O., & Isola, I. (2013, January). The intimate relationship between strain and magmatism: A numerical treatment of clustered monogenetic fields in the Main Ethiopian Rift. *Tectonics*, *32*(1), 49–64. Retrieved 2018-11-13, from http://doi.wiley.com/10.1029/2012TC003146 doi: 10.1029/2012TC003146

Mickus, K., Tadesse, K., Keller, G. R., & Oluma, B. (2007, June). Gravity analysis of the main Ethiopian rift. *Journal of African Earth Sciences*, *48*(2), 59–69. Retrieved 2021-11-30, from https://www.sciencedirect.com/science/article/pii/S1464343X07000192 doi: 10.1016/j.jafrearsci.2007.02.008

Moore, L. R., Gazel, E., Tuohy, R., Lloyd, A. S., Esposito, R., Steele-MacInnis, M., ... Bodnar, R. J. (2015, April). Bubbles matter: An assessment of the contribution of vapor bubbles to melt inclusion volatile budgets. *American Mineralogist*, *100*(4), 806–823. Retrieved 2019-05-13, from https://pubs.geoscienceworld.org/ammin/article/100/4/806-823/40390 doi: 10.2138/am-2015-5036

Moore, L. R., Mironov, N., Portnyagin, M., Gazel, E., & Bodnar, R. J. (2018, June). Volatile contents of primitive bubble-bearing melt inclusions from Klyuchevskoy volcano, Kamchatka: Comparison of volatile contents determined by mass-balance versus experimental homogenization. *Journal of Volcanology and Geothermal Research*, *358*, 124–131. Retrieved 2022-08-25, from https://www.sciencedirect.com/science/article/pii/S0377027317306510 doi: 10.1016/j.jvolgeores.2018.03.007

Muluneh, A. A., Brune, S., Illsley-Kemp, F., Corti, G., Keir, D., Glerum, A., ... Mori, J. (2020). Mechanism for Deep Crustal Seismicity: Insight From Modeling of Deformation Processes at the Main Ethiopian Rift. *Geochemistry, Geophysics, Geosystems*, *21*(7), e2020GC008935. Retrieved 2022-06-01, from https://onlinelibrary.wiley.com/doi/abs/10.1029/2020GC008935 (_eprint: https://onlinelibrary.wiley.com/doi/pdf/10.1029/2020GC008935) doi: 10.1029/2020GC008935

Muluneh, A. A., Keir, D., & Corti, G. (2021). Thermo-Rheological Properties of

the Ethiopian Lithosphere and Evidence for Transient Fluid Induced Lower Crustal Seismicity Beneath the Ethiopian Rift. *Frontiers in Earth Science*, *9*. Retrieved 2022-06-01, from https://www.frontiersin.org/article/10.3389/feart.2021.610165

Neave, D. A., Fabbro, G., Herd, R. A., Petrone, C. M., & Edmonds, M. (2012, March). Melting, Differentiation and Degassing at the Pantelleria Volcano, Italy. *Journal of Petrology*, *53*(3), 637–663. Retrieved 2019-02-05, from https://academic.oup.com/petrology/article/53/3/637/1613886 doi: 10.1093/petrology/egr074

Newman, S., & Lowenstern, J. B. (2002, June). VolatileCalc: a silicate melt–H_2O–CO_2 solution model written in Visual Basic for excel. *Computers & Geosciences*, *28*(5), 597–604. Retrieved 2021-02-01, from http://www.sciencedirect.com/science/article/pii/S0098300401000814 doi: 10.1016/S0098-3004(01)00081-4

Nicotra, E., Viccaro, M., Donato, P., Acocella, V., & De Rosa, R. (2021, November). Catching the Main Ethiopian Rift evolving towards plate divergence. *Scientific Reports*, *11*(1), 21821. Retrieved 2021-11-09, from https://www.nature.com/articles/s41598-021-01259-6 (Bandiera_abtest: a Cc_license_type: cc_by Cg_type: Nature Research Journals Number: 1 Primary_atype: Research Publisher: Nature Publishing Group Subject_term: Petrology;Tectonics;Volcanology Subject_term_id: petrology;tectonics;volcanology) doi: 10.1038/s41598-021-01259-6

Oliveira, M. E., Gomes, A. S., Rosas, F. M., Duarte, J. C., França, G. S., Almeida, J. C., & Fuck, R. A. (2022, May). Impact of crustal rheology and inherited mechanical weaknesses on early continental rifting and initial evolution of double graben structural configurations: Insights from 2D numerical models. *Tectonophysics*, *831*, 229281. Retrieved 2022-12-10, from https://www.sciencedirect.com/science/article/pii/S0040195122000750 doi: 10.1016/j.tecto.2022.229281

Rasmussen, D. J., Plank, T. A., Wallace, P. J., Newcombe, M. E., & Lowenstern, J. B. (2020, December). Vapor-bubble growth in olivine-hosted melt inclusions. *American Mineralogist*, *105*(12), 1898–1919. Retrieved 2021-03-03, from https://pubs.geoscienceworld.org/msa/ammin/article/105/12/1898/592851/Vapor-bubble-growth-in-olivine-hosted-melt (Publisher: GeoScienceWorld) doi: 10.2138/am-2020-7377

Reiss, M. C., De Siena, L., & Muirhead, J. D. (2022). The Interconnected Magmatic Plumbing System of the Natron Rift. *Geophysical Research Letters*, *49*(15), e2022GL098922. Retrieved 2022-11-24, from https://onlinelibrary.wiley.com/doi/abs/10.1029/2022GL098922 (_eprint: https://onlinelibrary.wiley.com/doi/pdf/10.1029/2022GL098922) doi: 10.1029/2022GL098922

Reiss, M. C., Muirhead, J. D., Laizer, A., Link, F., Kazimoto, E., Ebinger, C. J., & Rümpker, G. (2021, February). The Impact of Complex Volcanic Plumbing on the Nature of Seismicity in the Developing Magmatic Natron Rift, Tanzania. *Frontiers in Earth Science*, *8*. doi: 10.3389/feart.2020.609805

Rooney, T. O., Bastow, I. D., & Keir, D. (2011, April). Insights into extensional processes during magma assisted rifting: Evidence from aligned scoria cones. *Journal of Volcanology and Geothermal Research*, *201*(1), 83–96. Retrieved 2018-02-02, from http://www.sciencedirect.com/science/article/pii/S0377027310002386 doi: 10.1016/j.jvolgeores.2010.07.019

Rooney, T. O., Furman, T., Yirgu, G., & Ayalew, D. (2005, August). Structure of the Ethiopian lithosphere: Xenolith evidence in the Main Ethiopian Rift. *Geochimica et Cosmochimica Acta*, *69*(15), 3889–3910. Retrieved 2018-10-25, from http://www.sciencedirect.com/science/article/pii/S0016703705003042 doi: 10.1016/j.gca.2005.03.043

Rooney, T. O., Wallace, P. J., Muirhead, J. D., Chiasera, B., Steiner, R. A., Girard, G., & Karson, J. A. (2022, November). Transition to magma-driven rifting in the South Turkana Basin, Kenya: Part 2. *Journal of the Geological Society*, *179*(6), jgs2021–160. Retrieved 2022-10-31, from https://www.lyellcollection.org/doi/10.1144/jgs2021-160 doi: 10.1144/jgs2021-160

Saria, E., Calais, E., Stamps, D. S., Delvaux, D., & Hartnady, C. J. H. (2014, March). Present-day kinematics of the East African Rift. *Journal of Geophysical Research: Solid Earth*, *119*(4), 3584–3600. Retrieved 2018-11-01, from https://agupubs.onlinelibrary.wiley.com/doi/full/10.1002/2013JB010901 doi: 10.1002/2013JB010901

Schneider, C. A., Rasband, W. S., & Eliceiri, K. W. (2012, July). NIH Image to ImageJ: 25 years of image analysis. *Nature Methods*, *9*(7), 671–675. Retrieved 2021-03-17, from https://www.nature.com/articles/nmeth.2089 (Number: 7 Publisher: Nature Publishing Group) doi: 10.1038/nmeth.2089

Shishkina, T., Botcharnikov, R., Holtz, F., Almeev, R., & Portnyagin, M. (2010, October). Solubility of H_2O- and CO_2-bearing fluids in tholeiitic basalts at pressures up to 500MPa. *Chemical Geology*, *277*(1-2), 115–125. Retrieved 2021-09-10, from https://linkinghub.elsevier.com/retrieve/pii/S0009254110002640 doi: 10.1016/j.chemgeo.2010.07.014

Shorttle, O., & Maclennan, J. (2011, November). Compositional trends of Icelandic basalts: Implications for short–length scale lithological heterogeneity in mantle plumes. *Geochemistry, Geophysics, Geosystems*, *12*(11), Q11008. Retrieved 2017-02-01, from http://onlinelibrary.wiley.com/doi/10.1029/2011GC003748/abstract doi: 10.1029/2011GC003748

Tadesse, A. Z., Ayalew, D., Pik, R., Yirgu, G., & Fontijn, K. (2019, January). Magmatic evolution of the Boku Volcanic Complex, Main Ethiopian Rift. *Journal of African Earth Sciences*, *149*, 109–130. Retrieved 2019-01-26, from http://www.sciencedirect.com/science/article/pii/S1464343X18302450 doi: 10.1016/j.jafrearsci.2018.08.003

Tetreault, J. L., & Buiter, S. J. H. (2018, October). The influence of extension rate and crustal rheology on the evolution of passive margins from rifting to break-up. *Tectonophysics*, *746*, 155–172. Retrieved 2022-12-01, from https://www.sciencedirect.com/science/article/pii/S0040195117303505 doi: 10.1016/j.tecto.2017.08.029

Thybo, H., & Nielsen, C. A. (2009, February). Magma-compensated crustal thinning in continental rift zones. *Nature*, *457*(7231), 873–876. Retrieved 2018-05-23, from https://www.nature.com/articles/nature07688 doi: 10.1038/nature07688

Tucker, J. M., Hauri, E. H., Pietruszka, A. J., Garcia, M. O., Marske, J. P., & Trusdell, F. A. (2019, June). A high carbon content of the Hawaiian mantle from olivine-hosted melt inclusions. *Geochimica et Cosmochimica Acta*, *254*, 156–172. Retrieved 2019-05-15, from http://www.sciencedirect.com/science/article/pii/S001670371930208X doi: 10.1016/j.gca.2019.04.001

Wallace, P. J., Plank, T., Bodnar, R. J., Gaetani, G. A., & Shea, T. (2021). Olivine-Hosted Melt Inclusions: A Microscopic Perspective on a Complex Magmatic World. *Annual Review of Earth and Planetary Sciences*, *49*(1), null. Retrieved 2021-03-03, from https://doi.org/10.1146/annurev-earth-082420-060506 (_eprint: https://doi.org/10.1146/annurev-earth-082420-060506) doi: 10.1146/annurev-earth-082420-060506

Weinstein, A., Oliva, S. J., Ebinger, C. J., Roecker, S., Tiberi, C., Aman, M., ... Fischer, T. P. (2017). Fault-magma interactions during early continental rifting: Seismicity of the Magadi-Natron-Manyara basins, Africa. *Geochemistry, Geophysics, Geosystems*, *18*(10), 3662–3686. Retrieved 2022-11-24, from https://onlinelibrary.wiley.com/doi/abs/10.1002/2017GC007027

(_eprint: https://onlinelibrary.wiley.com/doi/pdf/10.1002/2017GC007027) doi: 10.1002/2017GC007027

Whaler, K. A., & Hautot, S. (2006, January). The electrical resistivity structure of the crust beneath the northern Main Ethiopian Rift. In G. Yirgu, C. J. Ebinger, & P. K. H. Maguire (Eds.), *The Afar Volcanic Province within the East African Rift System* (Vol. 259, pp. 293–305). Retrieved 2018-11-12, from http://sp.lyellcollection.org/content/259/1/293

White, R. S., Smith, L. K., Roberts, A. W., Christie, P. a. F., Kusznir, N. J., & the rest of the iSIMM Team. (2008, March). Lower-crustal intrusion on the North Atlantic continental margin. *Nature*, *452*(7186), 460–464. Retrieved 2018-05-13, from https://www.nature.com/articles/nature06687 doi: 10.1038/nature06687

Wieser, P. E., Iacovino, K., Matthews, S., Moore, G., & Allison, C. M. (2022). VESIcal: 2. A Critical Approach to Volatile Solubility Modeling Using an Open-Source Python3 Engine. *Earth and Space Science*, *9*(2), e2021EA001932. Retrieved 2022-07-14, from https://onlinelibrary.wiley.com/doi/abs/10.1029/2021EA001932 (_eprint: https://onlinelibrary.wiley.com/doi/pdf/10.1029/2021EA001932) doi: 10.1029/2021EA001932

Wieser, P. E., Lamadrid, H., Maclennan, J., Edmonds, M., Matthews, S., Iacovino, K., ... Ilyinskaya, E. (2021). Reconstructing Magma Storage Depths for the 2018 Kilauean Eruption From Melt Inclusion CO_2 Contents: The Importance of Vapor Bubbles. *Geochemistry, Geophysics, Geosystems*, *22*(2), e2020GC009364. Retrieved 2021-02-13, from https://agupubs.onlinelibrary.wiley.com/doi/abs/10.1029/2020GC009364 (_eprint: https://agupubs.onlinelibrary.wiley.com/doi/pdf/10.1029/2020GC009364) doi: https://doi.org/10.1029/2020GC009364

Wong, K., Ferguson, D., Matthews, S., Morgan, D., Tadesse, A. Z., Sinetebeb, Y., & Yirgu, G. (2022, November). Exploring rift geodynamics in Ethiopia through olivine-spinel Al-exchange thermometry and rare-earth element distributions. *Earth and Planetary Science Letters*, *597*, 117820. Retrieved 2022-09-23, from https://www.sciencedirect.com/science/article/pii/S0012821X22004563 doi: 10.1016/j.epsl.2022.117820

References from the Supporting Information

(Schneider et al., 2012; Tucker et al., 2019; Wieser et al., 2021; Lamadrid et al., 2017; Hartley et al., 2014; Iacovino & Till, 2019; Moore et al., 2018, 2015; DeVitre et al., 2021; Hauri et al., 2002; Shishkina et al., 2010; Jochum et al., 2006; Jarosewich, 2002; J. J. Donovan, 2021; Danyushevsky & Plechov, 2011; Danyushevsky, 2001; Gleeson et al., 2017; DeVitre et al., 2022; Iacovino et al., 2021; Wieser et al., 2022; Ghiorso & Gualda, 2015; Iddon et al., 2019; Wong et al., 2022; Iddon & Edmonds, 2020; Dixon, 1997; Iacono-Marziano et al., 2012; Allison et al., 2019; Newman & Lowenstern, 2002; Gualda et al., 2012; Neave et al., 2012; Blundy & Wood, 1991; Saria et al., 2014; Le Voyer et al., 2018; Kendall et al., 2005; Bastow et al., 2010; Lavayssière et al., 2018; Daniels et al., 2014; Armitage et al., 2015; Hunt et al., 2017; Keir et al., 2006; Daly et al., 2008)

CReDiT: Author Contributions

- Conceptualization: KW, DF, DM, ME, GY
- Formal analysis: KW, DF, PW, ME
- Funding acquisition: KW, DF, DM, ME, GY
- Investigation: KW, DF, PW, JH, SH
- Resources: KW, DF, AZT, GY
- Supervision: DF, DM, ME, GY
- Visualization: KW, PW
- Writing – original draft: KW, DF
- Writing – review and editing: All authors

Figure 1.

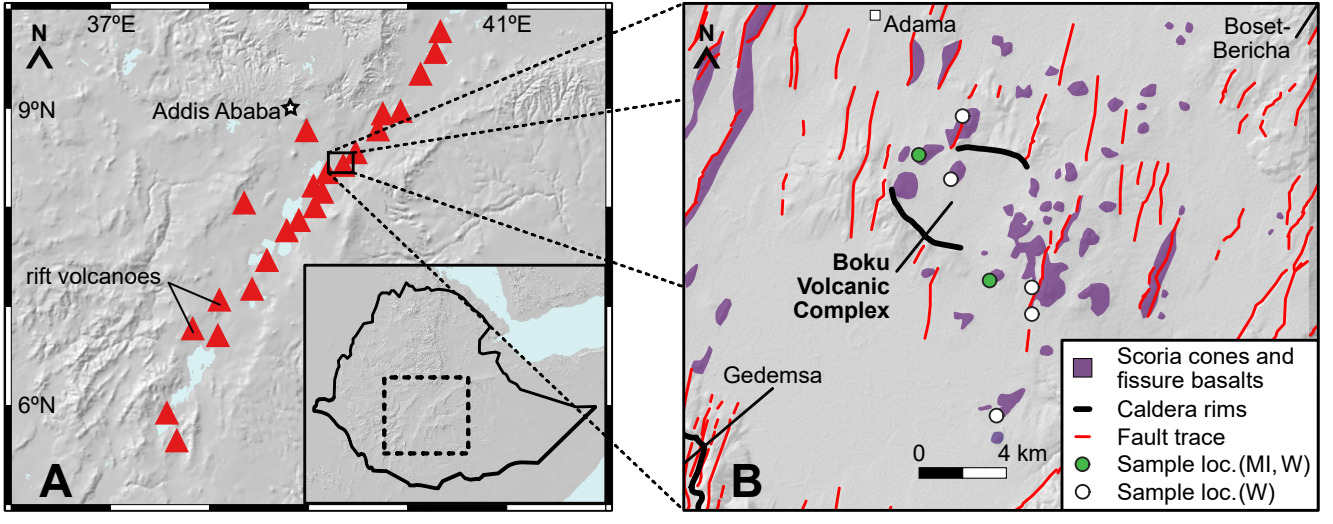
N
37ºE
41ºE
9ºN
Addis Ababa
rift volcanoes
6ºN
A
N
Adama
Boset-
Bericha
Boku
Volcanic
Complex
Gedemsa
B
0
4 km
Scoria cones and
fissure basalts
Caldera rims
Fault trace
Sample loc. (MI, W)
Sample loc. (W)

Figure 2.

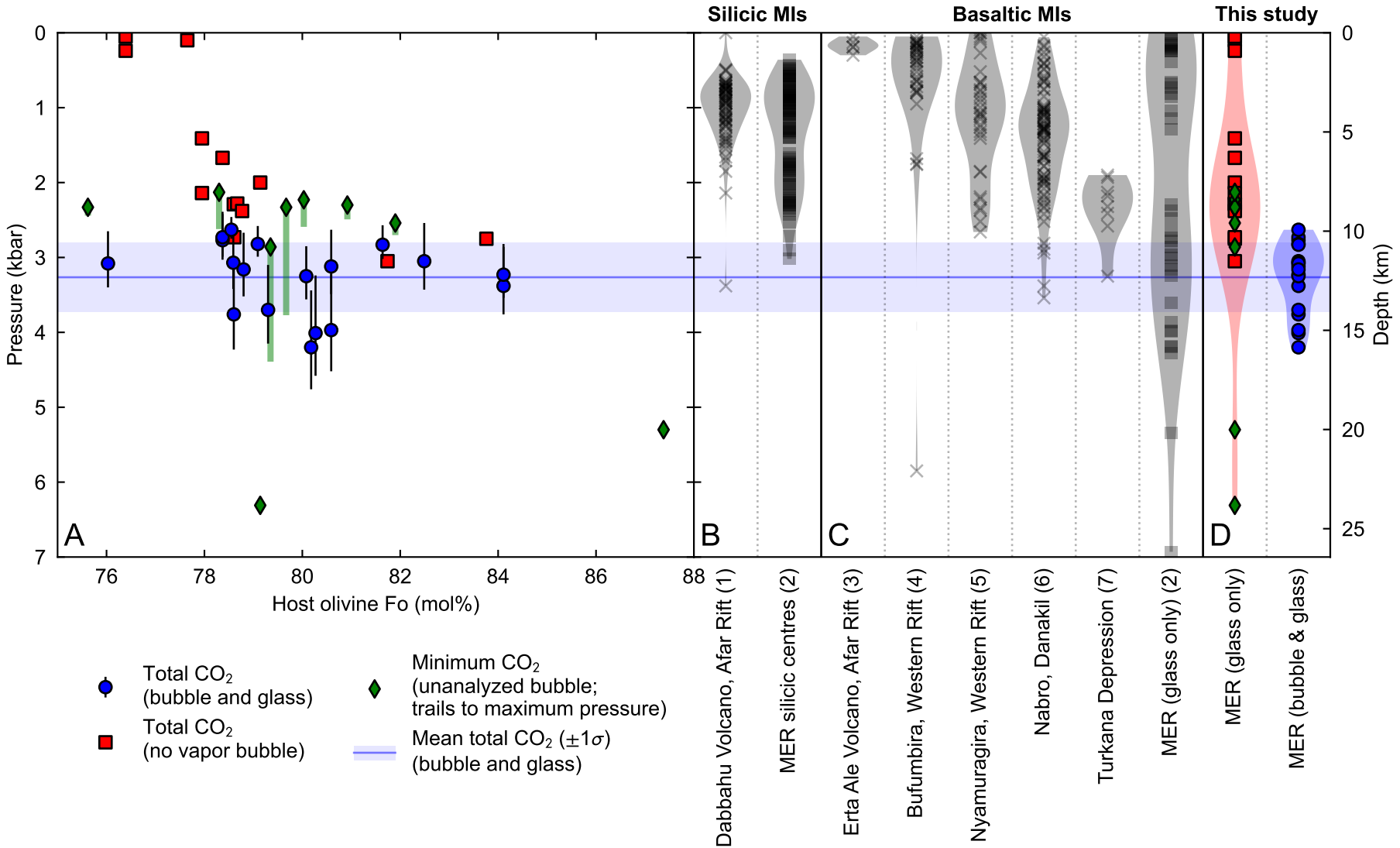
Silicic MIs
Basaltic MIs
This study
Pressure (kbar)
Depth (km)
Host olivine Fo (mol%)
A
B
C
D
Dabbahu Volcano, Afar Rift (1)
MER silicic centres (2)
Erta Ale Volcano, Afar Rift (3)
Bufumbira, Western Rift (4)
Nyamuragira, Western Rift (5)
Nabro, Danakil (6)
Turkana Depression (7)
MER (glass only) (2)
MER (glass only)
MER (bubble & glass)
Total CO2 (bubble and glass)
Total CO2 (no vapor bubble)
Minimum CO2 (unanalyzed bubble; trails to maximum pressure)
Mean total CO2 (±1σ) (bubble and glass)

Figure 3.

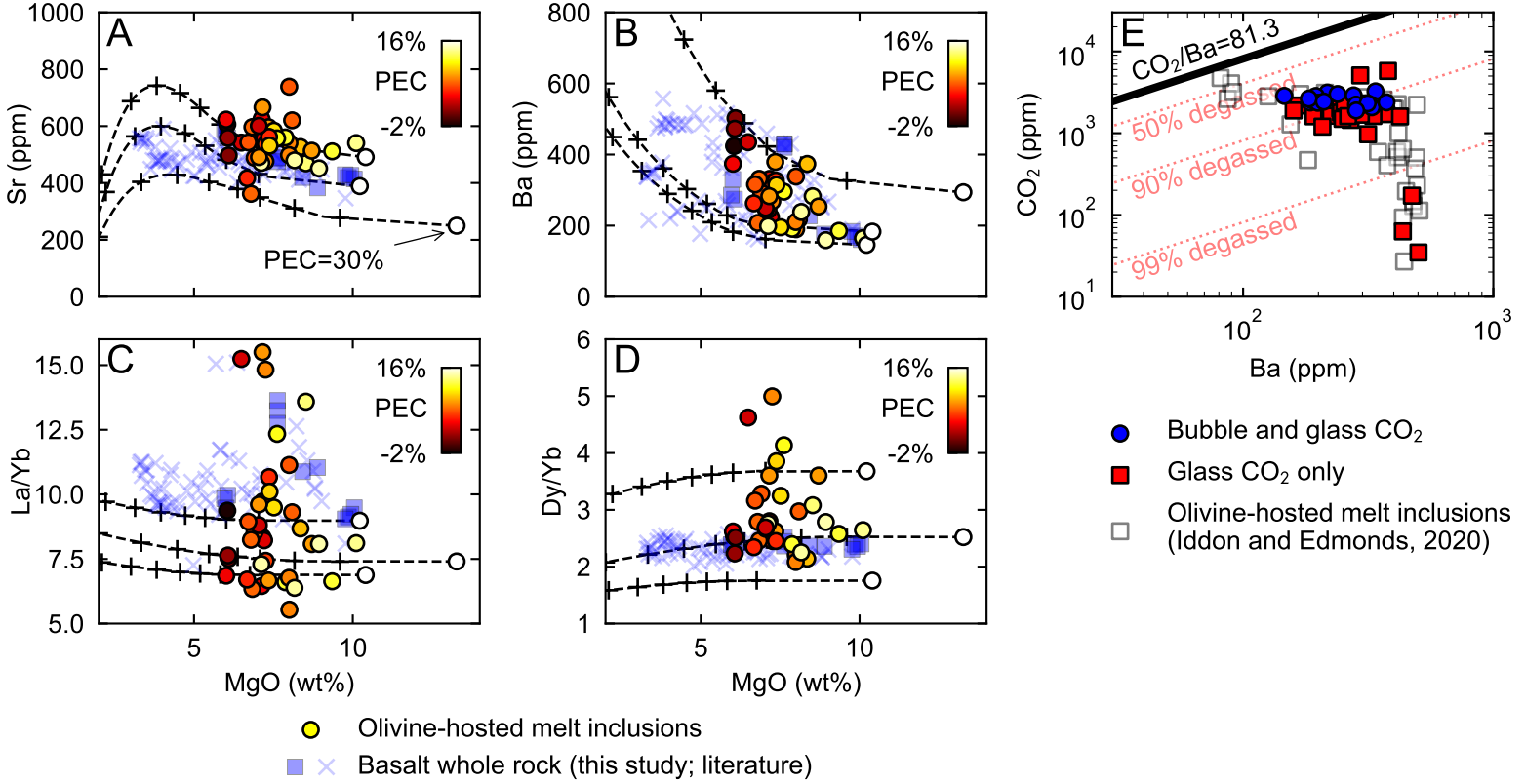
A
B
C
D
E
16%
PEC
-2%
PEC=30%
Sr (ppm)
Ba (ppm)
La/Yb
Dy/Yb
MgO (wt%)
CO2 (ppm)
CO2/Ba=81.3
50% degassed
90% degassed
99% degassed
Bubble and glass CO2
Glass CO2 only
Olivine-hosted melt inclusions
(Iddon and Edmonds, 2020)
Olivine-hosted melt inclusions
Basalt whole rock (this study; literature)

Figure 4.

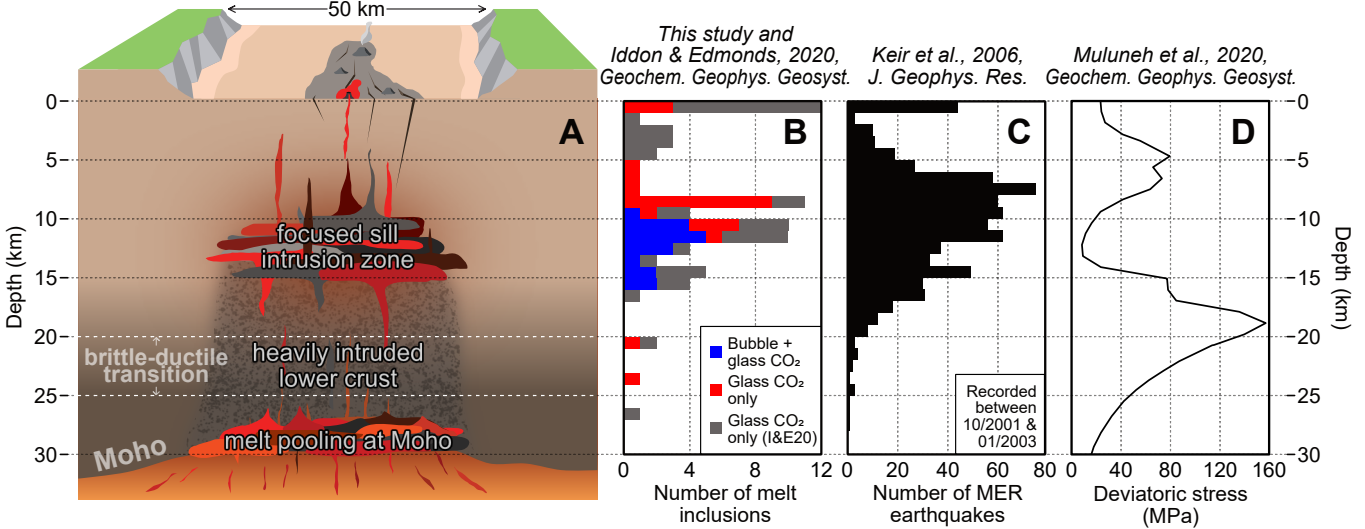
50 km
A
focused sill intrusion zone
brittle-ductile transition
heavily intruded lower crust
melt pooling at Moho
Moho
Depth (km)
0
5
10
15
20
25
30
This study and Iddon & Edmonds, 2020, Geochem. Geophys. Geosyst.
B
Bubble + glass CO₂
Glass CO₂ only
Glass CO₂ only (I&E20)
0
4
8
12
Number of melt inclusions
Keir et al., 2006, J. Geophys. Res.
C
Recorded between 10/2001 & 01/2003
0
20
40
60
80
Number of MER earthquakes
Muluneh et al., 2020, Geochem. Geophys. Geosyst.
D
0
40
80
120
160
Deviatoric stress (MPa)
Depth (km)